A KINEMATIC ANALYSIS OF A STACKED PLANAR COMPLIANT TENSEGRITY MECHANISM

by

MIRANDA TANOUYE

VISHESH VIKAS, COMMITTEE CHAIR
KEITH WILLIAMS
SAMEER MULANI

A THESIS

Submitted in partial fulfillment of the requirements
for the degree of Master of Science
in the Department of Mechanical Engineering
in the Graduate School of
The University of Alabama

TUSCALOOSA, ALABAMA

2019

ABSTRACT

Traditional tensegrity mechanisms are comprised of compressive (rigid rods) and tensile members (strings). Compliant tensegrity mechanisms (CoTM) introduce springs alongside strings and rods, allowing these structures to be more adaptable and robust. The kinematic and stability analyses of such mechanisms will facilitate better behavioral understanding for control of such structures. Such structures are known to display nonlinear behaviors including multiple equilibria. Previously, a simple planar model of such a CoTM has been studied. This can be furthered upon by viewing the mechanism as a single link within a kinematic chain. However, a nomenclature methodology for kinematic chain of CoTM modules is lacking. The equilibrium analysis of CoTM is non-trivial as the equilibrium equations are nonlinear in variables (angles occuring as sine and cosine). Mathematically, for a small number of equations, the solutions can be obtained using polynomial elimination methods. The computational complexity increases exponentially with the number of equations along with the number of equilibrium solutions.

The presented work analyzes single module and chain of planar CoTM comprising of two rigid bodies connected by a rigid link and two springs through revolute joints. The computational complexity of a planar CoTM link increases drastically as the zero free-length (ZFL) constraint of the springs in relaxed. Stability of the solutions is evaluated by observing the eigenvalues of the Jacobian of the equilibrium equations. After analyzing the system for one link, a two-link chain system is analyzed. Analysis is done based on knowledge gained from analyzing a single link and solving for all solutions of the mechanism and then determining stability of the found equilibrium solutions.

DEDICATION

I would like to dedicate this body of work to all my friends and family who have supported me throughout this whole endeavor. This would not be possible without your love and guidance, especially my parents and siblings for their support going through these six years of school. Thank you all for trying to understand and willingness to listen to my rants.

LIST OF ABBREVIATIONS AND SYMBOLS

CoTM	Compliant Tensegrity Mechanism
DCE	Displacement Constraint Equation
DH	Denavit-Hartenberg Parameters
DOF	Degree of Freedom
EE	Equilibrium Equation
$P_{i \to j}$	Displacement vector from point i to j
TCE	Trigonometric Constraint Equation
ZFL	Zero Free Length

ACKNOWLEDGMENTS

There are many people who have had a hand in this work, and I am so grateful to take this opportunity to thank them for their help. Overall, I am most grateful for the help Vishesh Vikas has provided over the years as my advisor by providing his wisdom and knowledge. I would also like to thank the rest of the members of my committee, Keith Williams and Sameer Mulani for their expertise and aid. Also, thank you to Beth Todd for her guidance and advice throughout my entire career here at the University. Without her wisdom I would not be here. Then also to Steve Shepard, for his honesty and answering all my questions on navigating graduate school. Finally, thank you to my fellow graduate students David Leech and Adrian Alegre. Without you both, I would not have made it.

CONTENTS

LIST OF TABLES

LIST OF FIGURES

CHAPTER 1

INTRODUCTION

Tensegrity mechanisms are made up of compressive and tensile members where no pair of struts touch and each end is connected to three non-coplanar ties. This provides some unique features: strain is distributed through deformation of the structure, they expand in all axes at once, and can be built from one another. These unique properties make them useful in the fields of robotics, space, bridges and biological modeling. Several natural structures can be modeled as a tensegrity mechanism, such as the human spine and DNA molecules. Their ability to withstand large amounts of strain and efficient packing (occupying less volume for storage) make them ideal for deployment applications.

Static, dynamic and stability analysis of these mechanisms provide insight into their behavior. The direct static problem yields equilibrium equations which are non-linear in the angle, thus, yielding multiple equilibrium solutions. The analytical solution structure of these equations is helpful in specifying the upper bound on the number of possible solutions. Some analytical solutions for prestressed tensegrity structures have been proposed and explored.

Compliant Tensegrity Mechanisms (CoTM) augment traditional tensegrity structures by adding spring elements that can both compress and extend. Moreover, the orientation of the mechanism may be controlled through its compliance, such as, by indirectly varying free lengths of the spring elements. Such modifications have been experimentally introduced to build tensegrity robots, however, their kinematic analysis has been limited. Initial research has explored the effect of variation of spring free lengths on the static

equilibrium and stability of a single link planar tensegrity mechanism. The presented research builds on these results to investigate static equilibrium and stability of a multi-link, stacked, system. Analysing the kinematics of these structures and observing how varying free lengths of the spring elements effects orientation and stability provides insight to their nature. As this is of more interest for future applications, such as for building larger structures or control of them.

Transitioning from a single-link to a multi-link , stacked, system requires modification in defining parameters, as certain components are now combined when stacked. However, the way all points are defined and called remains the same. A single-link is described by two angles, which define the orientation of the top rigid body and rigid rod with regard to the bottom rigid body. Meaning that the whole system is defined by the reference frame of the bottom rigid body. When stacking for multi-link mechanisms this remains the same, however their are now middle rigid bodies which are the combination of the top and bottom rigid bodies from separate links that are stacked on one another. The entire mechanism is still described by two angles for each link in the chain in the reference frame of the bottom rigid body. Now the difference is how the reference frame for the middles bodies is defined. All of this is explained in detail in Section 3 along with how the equilibrium equations are established for a single-link and two-link mechanism.

The static equilibrium and constraint equations for CoTM links are set of polynomial equations. Polynomial elimination methods are useful in obtaining analytical solutions for such systems. The single link system can be solved by constructing the Sylvester Matrix. However, these analytical methods become computationally expensive as the number of polynomial equations and variables increase, hence are not viable for multi-link systems. For such larger systems, numerical homotopy continuation methods are useful. Homotopy continuation methods are the primary computational methods used for numerical algebraic geometry and it creates a homotopy between polynomial systems. According to Bertini's theorem, homotopy continuation will theoretically compute all solutions of a system. The

Bertini software [2] developed by a group at the University of Notre Dame is an example of a numerical homotopy continuation methods solver suited for solving these static equilibrium equations.

The work described in this thesis proposes a methodology for describing these mechanism to facilitate simpler understanding and presentation. It hopes to provide a deeper insight into how and why these mechanisms move the way they do.

CHAPTER 2

LITERATURE REVIEW

Tensegrity mechanisms are seen applied to fields of space and robotics [23], biological modeling [13, 17, 18] and construction of bridges [3, 24]. They are adaptive and able to withstand high amounts of strain by distributing it across their bodies [21], and compact - they can easily be disassembled, condensed and then reassembled when ready for use as they are essentially made up of a network of strings and rigid rods. These make them attractive candidates for space applications and self-assembling deployable structures such as antennas [8, 9].

Several studies have discussed the build and analysis of tensegrity mechanisms [4, 5, 19, 25]. One major study in particular was done by a research group at NASA Ames where they had an initial study fabricating a regular tensegrity mechanism and then used the knowledge gained to build a compliant tensegrity mechanism. Similar studies like this have been conducted, but the issues seen are that they are able to build these mechanisms but don't go into detail for the kinematic analysis of such mechanisms. Their build and construction is done based on experimentation. For their work it is fine, but for advancement of the field and deeper understanding, computational analysis is key among a broad spectrum and in a less specific format.

Static analysis of tensegrity frameworks has been comprehensively investigated. Arsenault et al. [1] study the static and dynamic analysis of a two degree of freedom (DOF) planar tensegrity mechanism by analyzing the energy of the system, however, do not consider the stability of the system. While Juan et al. [15] discuss the rigidity and stability

of tensegrity structures from three different views: motions, forces and energy approaches. Defining the structure using a motion approach relies on rigidity, or absence of relative motion between members, and implies that the members of the framework are kept constant. The structure must maintain generic rigidity however for tensegrity frameworks this is not guaranteed, and additional conditions are required to do so. For a forces approach, the structure must be in equilibrium to maintain a rigid configuration. Analysing tensegrity structures using an energy approach looks at how the energy in the strings and struts changes as they are stretched or compressed.

Locomotion and control of non-compliant tensegrity mechanisms have been researched. Some have attempted locomotion by crawling or rolling [14, 22]. Crawling or rolling is achieved through displacement of the center of mass by lengthening or shortening the strings which cause the mechanism to fall over. However, such control methods are ad-hoc and not model-based. Since the mechanisms are non-compliant, their geometry is limited much more and makes them easier to solve. However, most studies do not investigate the kinematics of the mechanism. Paul et al. [20] provides in depth dynamic analysis for a three and four strut non-compliant tensegrity mechanism. Several have worked on the locomotion of tensegrity structures as well as simulations. One of the best known simulators is the NASA Tensegrity Robotics Toolkit (NTRT). It has been used in several studies to provide simulations of different configurations and parameters [10],[11].

Polynomial elimination methods are used to find solutions of a set of polynomial equations in multiple variables. Kapur provides several methods and understanding on their uses in [16]. As stated earlier, Sylvester's Matrix was the analytical method used for a single link system but as described by Kapur after a certain point it is no longer a viable method. This method can be used to solve larger systems, however it does so by eliminating several variables successively. Thus, this method has an explosive growth in the degrees of the polynomials that are generated from these successive eliminations which makes it impractical for eliminating more than three variables. Which is why for the sin-

gle link system, the Sylvester Matrix was only applicable when assuming both or one of the springs in the system were of zero free length (ZFL) since each non-ZFL spring adds one constraint equation. This is a method used in previous studies to simplify the analysis of compliant tensegrity structures, which include spring elements [6]. Zero free length is used in calculations by setting the free length of a spring equal to zero, and Delissen et. al. describes the design of such springs in [7].

CHAPTER 3

PROBLEM DEFINITION

3.1 SINGLE LINK COMPLIANT TENSEGRITY MECHANISM

The proposed mechanism is comprised of two rigid bodies connected by a compressive member and two spring elements as shown in Figure 3.1. Let coordinate systems T, B be fixed in reference frames of top and bottom rigid bodies respectively. The origin of B is P_1 and the x-axis is along vecotr $P_{1\rightarrow 2}$ and z-axis is out of plane of the paper. Origin of T is P_4 and the x-axis along vecotr $P_{4\rightarrow 6}$ and z-axis out of plane of the paper. The transformation matrix ${}^{T}_{B}T$ between coordinate system T and B is written as

$$ {}^{T}_{B}T = \begin{bmatrix} c_2 & -s_2 & 0 & L_3 c_1 \\ s_2 & c_2 & 0 & L_3 s_1 \\ 0 & 0 & 1 & 0 \\ 0 & 0 & 0 & 1 \end{bmatrix} \tag{3.1} $$

where c_i, s_i are $cos(\gamma_i)$ and $sin(\gamma_i)$ respectively.

The objective is to find the stable equilibrium configurations of the mechanism defined by angles γ_1 (angle between the x-axis of coordinate system B and the compressive member) and γ_2 (angle between the x-axes of coordinate systems B and T) for a given set of

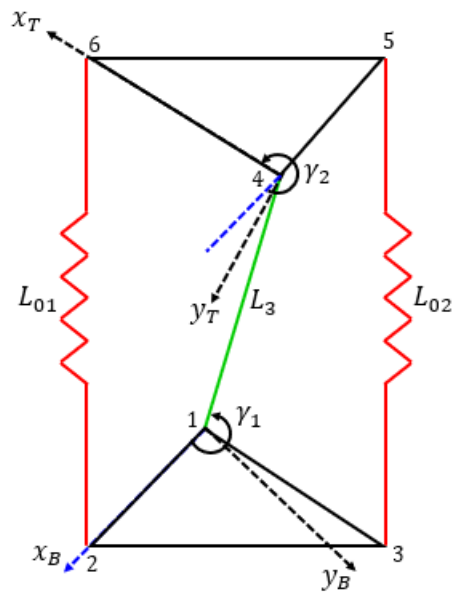

Figure 3.1: Single link of the proposed planar CoTM

parameters. A single-link system is referred to by

$$\gamma_1, \gamma_2 \rightarrow \text{state (orientation)}$$

$$L_{01}, L_{02} \rightarrow \text{control}$$

$$L_3, p_{i\rightarrow j} \rightarrow \text{system (rigid body parameters)}$$

Equilibrium Analysis After defining the overall mechanism in the bottom coordinate system, the overall Equilibrium Equations (EE) of the system can be defined as

$$E = F_1 + F_2 + F_3 = 0 \tag{3.2}$$

$$\tau = P_{1\rightarrow 2} \times F_2 + P_{1\rightarrow 3} \times F_3 = 0 \tag{3.3}$$

where F_i are defined as

$$F_1 = f_3 \left(\frac{P_{1\to4}}{L_3} \right) \tag{3.4}$$

$$F_2 = k_1(d_1 - L_{01}) \frac{P_{2\to6}}{d_1} \tag{3.5}$$

$$F_3 = k_2(d_2 - L_{02}) \frac{P_{3\to5}}{d_2} \tag{3.6}$$

where f_3 is the unknown force in the compressive bar and $f_i = k_i(d_i - L_{0i})$, $i = 1, 2$ are the forces in the spring elements such that d_i and L_{0i} are the overall length and free lengths of the spring element respectively. The free lengths can be thought of as a combination of the actual free length of the spring plus the length of the string element.

To simplify the system and eliminate the unknown compressive force f_3, Equation 3.2 is crossed with $P_{1\to4}$, creating a new equilibrium equation. Now, the four equations of interest are the two Equilibrium Equations (EE)

$$\begin{aligned} E_{new} &= P_{1\to4} \times F_2 + P_{1\to4} \times F_3 \\ &= k_1(1 - \frac{L_{01}}{d_1})(P_{1\to4} \times P_{2\to6}) + k_2(1 - \frac{L_{02}}{d_2})(P_{1\to4} \times P_{3\to5}) = 0 \qquad (3.7) \\ \tau &= k_1(1 - \frac{L_{01}}{d_1})(P_{1\to2} \times P_{2\to6}) + k_2(1 - \frac{L_{02}}{d_2})(P_{1\to3} \times P_{3\to5}) = 0 \qquad (3.8) \end{aligned}$$

As well as two Displacement Constraint Equations (DCE), which take into consideration parameters d_1 and d_2 that are constrained by the length of vectors $P_{2\to6}$ and $P_{3\to5}$ respectively.

$$d_1^2 - \|P_{2\to6}\|^2 = 0 \tag{3.9}$$

$$d_2^2 - \|P_{3\to5}\|^2 = 0 \tag{3.10}$$

From here, the system can then be solved using the numerical polynomial solver called Bertini^{TM}. Since Bertini^{TM}can only solve for a system of polynomial equations, c_i, s_i are

left as constants in the equations and not treated as trigonometric equations. This however requires two Trigonometric Constraint Equations (TCE) to account for the fact that they are dependent on one another.

$$c_1^2 + s_1^2 - 1 = 0 \tag{3.11}$$

$$c_2^2 + s_2^2 - 1 = 0 \tag{3.12}$$

	Equations	Unknowns
EE	E_{new} τ	c_i, s_i, d_i for $i = 1, 2$
DCE	d_1 d_2	c_i, s_i for $i = 1, 2$
TCE	c_1, s_1 c_2, s_2	-

Table 3.1: List of equations for a single link CoTM and their respective unknowns

Stability Analysis Determining the stability of an equilibrium point in a system requires observing how it reacts when some some disturbance is applied at the point of interest. The Taylor Series expansion for a given perturbation ∂y to a system $f(x)$ about an equilibrium point x_0 is

$$f(x_0 + \partial y) = f(x_0) + \left.\frac{\partial f(x)}{\partial y}\right|_{x=x_0} \partial y + \frac{1}{2!}\left.\frac{\partial^2 f(x)}{\partial y^2}\right|_{x=x_0} \partial y^2 + \dots$$

where the higher order terms can be ignored if the region of operation is near x_0, implying

$$\delta f(x_0) = \underbrace{\left.\frac{\partial f(x)}{\partial y}\right|_{x=x_0}}_{J_y} \delta y \tag{3.13}$$

This system will converge (become stable) if the real part of the eigenvalues of the Jacobian lie are negatuve i.e. $Re\{\text{eig}[J_y]\} < 0$, where J_y is the Jacobian. For this study, angular disturbance is of interest, hence, the Jacobian is taken with respect to the two angles

of the system (γ_1, γ_2) and is constructed as seen below where Z_x implied $\frac{\partial Z}{\partial x}$.

$$J_\gamma(x_0) = \left.\begin{bmatrix} F_{\gamma_1} & F_{\gamma_2} \\ \tau_{\gamma_1} & \tau_{\gamma_2} \end{bmatrix}\right|_{x=x_0} \tag{3.14}$$

The eigenvalues of this Jacobian are evaluated for each equilibrium solution, and the point is considered stable if all $Re\{\text{eig}[J_\gamma]\} < 0$.

3.2 TWO LINKS

Section 3.1 described the proposed mechanism as a single link, this section considers the mechanism as a stacked system, using a two link mechanism as an example which is shown in Figure 3.2. The mechanism is comprised of three rigid bodies, two compressive members and four spring elements. The top rigid body of link one and bottom rigid body of link two are considered as one rigid body for the stacked system.

Each of the rigid bodies define a coordinate system: bottom, B, middle, M, and top, T. System B has origin at P_1 with x-axis along vector $P_{1\to2}$, system M has origin at P_4 with x-axis along vector $P_{4\to7}$, and system T has origin at P_{10} with x-axis along vector $P_{10\to12}$. All z-axes are out of plane of the paper. Similarly to the single link mechanism, the M and T systems are translated to the B system with transformation matrices ${}^M_BT$ and ${}^T_BT$ respectively

$${}^M_BT = \begin{bmatrix} c_2 & -s_2 & 0 & L_1c_1 \\ s_2 & c_2 & 0 & L_1s_1 \\ 0 & 0 & 1 & 0 \\ 0 & 0 & 0 & 1 \end{bmatrix} \tag{3.15}$$

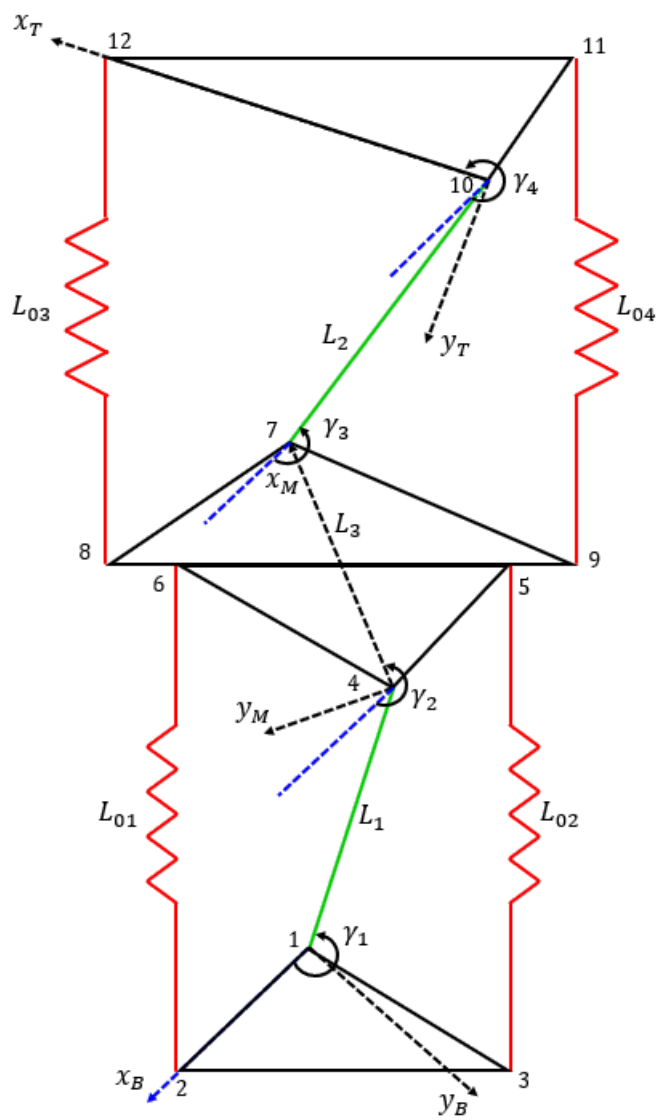

Figure 3.2: Two link stacked chain of the proposed planar CoTM

$$
{}^{T}_{B}T = \begin{bmatrix} c_4 & -s_4 & 0 & L_1c_1 + L_3c_2 + L_2c_3 \\ s_4 & c_4 & 0 & L_1s_1 + L_3s_2 + L_2s_3 \\ 0 & 0 & 1 & 0 \\ 0 & 0 & 0 & 1 \end{bmatrix} \tag{3.16}
$$

Where L_1 and L_2 are the distances of the rigid members, or the distance of vectors $P_{1\to4}$ and $P_{7\to10}$ respectively. L_3 is the distance from P_4 to P_7. There are four angles that

define the orientation of the entire mechanism, γ_1 is defined as the angle between the x-axis of the bottom B system and L_1, γ_2 is the angle from the x-axis of the bottom B system to the x-axis of the middle M system, γ_3 is the angle from the x-axis of the middle M system to L_2 and γ_4 is the angle from the x-axis of the bottom B system to the x-axis of the top T system.

Equilibrium Analysis The overall system has six equilibrium equations, an overall force and torque equation for each of the three bodies. The EE are shown below

$$\sum E_B = F_1 + F_2 + F_3 = 0 \tag{3.17}$$

$$\sum \tau_B = P_{1\to2} \times F_2 + P_{1\to3} \times F_3 = 0 \tag{3.18}$$

$$\sum E_M = F_4 + F_5 + F_6 + F_7 + F_8 + F_9 = 0 \tag{3.19}$$

$$\sum \tau_M = P_{4\to5} \times F_5 + P_{4\to6} \times F_6 + P_{4\to7} \times F_7 + P_{4\to8} \times F_8 + P_{4\to9} \times F_9 = 0 \tag{3.20}$$

$$\sum E_T = F_{10} + F_{11} + F_{12} = 0 \tag{3.21}$$

$$\sum \tau_T = P_{10\to11} \times F_{11} + P_{10\to12} \times F_{12} = 0 \tag{3.22}$$

such that F_i are defined as

$$F_1 = f_1 \frac{P_{1\to4}}{L_1} \tag{3.23}$$

$$F_2 = k_1(d_1 - L_{01})\frac{P_{2\to6}}{d_1} \tag{3.24}$$

$$F_3 = k_2(d_2 - L_{02})\frac{P_{3\to5}}{d_2} \tag{3.25}$$

$$F_4 = f_1 \frac{P_{4\to1}}{L_1} \tag{3.26}$$

$$F_5 = k_2(d_2 - L_{02})\frac{P_{5\to3}}{d_2} \tag{3.27}$$

$$F_6 = k_1(d_1 - L_{01})\frac{P_{6\to2}}{d_1} \tag{3.28}$$

$$F_7 = f_2 \frac{P_{7\to10}}{L_2} \tag{3.29}$$

$$F_8 = k_3(d_3 - L_{03})\frac{P_{8\to12}}{d_3} \tag{3.30}$$

$$F_9 = k_4(d_4 - L_{04})\frac{p_{9\to11}}{d_4} \tag{3.31}$$

$$F_{10} = f_2 \frac{P_{10\to7}}{L_2} \tag{3.32}$$

$$F_{11} = k_4(d_4 - L_{04})\frac{P_{11\to9}}{d_4} \tag{3.33}$$

$$F_{12} = k_3(d_3 - L_{03})\frac{P_{12\to8}}{d_3} \tag{3.34}$$

where f_1 and f_2 are the forces from the two compressive members. To eliminate the unknown compressive forces f_1, f_2, Equations 3.17 and 3.21 are crossed with $P_{1\to4}$ and $P_{7\to10}$ respectively.

$$\begin{aligned} E_{Bnew} &= E_B \times P_{1\to4} = P_{1\to4} \times F_2 + P_{1\to4} \times F_3 \\ &= k_1(1 - \frac{L_{01}}{d_1})(P_{1\to4} \times P_{2\to6}) + k_2(1 - \frac{L_{02}}{d_2})(P_{1\to4} \times P_{3\to5}) = 0 \end{aligned} \tag{3.35}$$

$$\begin{aligned} E_{Tnew} &= E_T \times P_{7\to10} = P_{7\to10} \times F_{11} + P_{7\to10} \times F_{12} \\ &= k_4(1 - \frac{L_{04}}{d_4})(P_{7\to10} \times P_{11\to9}) + k_3(1 - \frac{L_{03}}{d_3})(P_{7\to10} \times P_{12\to8}) = 0 \end{aligned} \tag{3.36}$$

There is no new E_M equation because the equilibrium and torque equations for the middle body are not used in the final system of equations. This is due in part because it is difficult to eliminate both f_1 and f_2 from Equations 3.19 and 3.20 but mostly because it would make the system over defined. By simplifying the system and eliminating f_1, f_2 there are now only 12 unknowns, c_i, s_i, d_i for $i = 1, 2, 3, 4$.

Also, there are now four DCE in comparison to two for a single link due to the addition of two more spring elements

$$d_1^2 - \|P_{2\to 6}\|^2 = 0 \tag{3.37}$$

$$d_2^2 - \|P_{3\to 5}\|^2 = 0 \tag{3.38}$$

$$d_3^2 - \|P_{8\to 12}\|^2 = 0 \tag{3.39}$$

$$d_4^2 - \|P_{9\to 11}\|^2 = 0 \tag{3.40}$$

Since there are two angles that define the orientation of each link, now four angles define the orientation of this two link stacked system and four TCE shown below

$$c_1^2 + s_1^2 - 1 = 0 \tag{3.41}$$

$$c_2^2 + s_2^2 - 1 = 0 \tag{3.42}$$

$$c_3^2 + s_3^2 - 1 = 0 \tag{3.43}$$

$$c_4^2 + s_4^2 - 1 = 0 \tag{3.44}$$

Including the equilibrium and torque equations on the middle rigid body would make the system then have 14 total equations. This overdefines the system and so the equations for the middle rigid body are not included.

Now the mechanism can be defined using 12 unknowns ($c_i, s_i, d_i \forall i = 1, \cdots, 4$) and 12 equations. The equations include the force and torque equations for the top and bottom rigid bodies (Equations 3.35, 3.36, 3.18, 3.22) and the eight constraint equations (Equa-

tions 3.37 through 3.44).

Similar to Section 3.1, the system is solved for using the numerical polynomial solver Bertini using the mentioned equations for a given set of unknown parameters. Since the system is non-linear there are several solutions for each parameter set.

	Equations	Unknowns
EE	E_{Bnew}	c_i, s_i, d_i for $i = 1, 2$
	τ_B	
	E_{Tnew}	c_i, s_i, d_i for $i = 1 \ldots 4$
	τ_T	
DCE	d_1	c_i, s_i for $i = 1, 2$
	d_2	
	d_3	c_i, s_i for $i = 1 \ldots 4$
	d_4	
TCE	c_1, s_1	-
	c_2, s_2	
	c_3, s_3	
	c_4, s_4	

Table 3.2: List of equations for a two link chain CoTM and their respective unknowns

Stability Analysis The main interest of this study is the stability of these equilibrium solutions, which is determined by evaluating the eigenvalues of the Jacobian for each solution. The Jacobian can be taken in reference to either the free lengths, L_{0i}, or the angles, γ_i. Equations 3.45 and 3.46 show the constructed Jacobian for each case. For this study, the stability is determined by the second Jacobian as it is more robust. When taken in reference to the free lengths, the situation becomes dynamic and for this study only the static case is of interest.

$$J_{L_0} = \begin{bmatrix} E_{B_{L_{01}}} & E_{B_{L_{02}}} & E_{B_{L_{03}}} & E_{B_{L_{04}}} \\ \tau_{B_{L_{01}}} & \tau_{B_{L_{02}}} & \tau_{B_{L_{03}}} & \tau_{B_{L_{04}}} \\ E_{T_{L_{01}}} & E_{T_{L_{02}}} & E_{T_{L_{03}}} & E_{T_{L_{04}}} \\ \tau_{T_{L_{01}}} & \tau_{T_{L_{02}}} & \tau_{T_{L_{03}}} & \tau_{T_{L_{04}}} \end{bmatrix} \tag{3.45}$$

$$J_\gamma = \begin{bmatrix} E_{B_{\gamma_1}} & E_{B_{\gamma_2}} & E_{B_{\gamma_3}} & E_{B_{\gamma_4}} \\ \tau_{B_{\gamma_1}} & \tau_{B_{\gamma_2}} & \tau_{B_{\gamma_3}} & \tau_{B_{\gamma_4}} \\ E_{T_{\gamma_1}} & E_{T_{\gamma_2}} & E_{T_{\gamma_3}} & E_{T_{\gamma_4}} \\ \tau_{T_{\gamma_1}} & \tau_{T_{\gamma_2}} & \tau_{T_{\gamma_3}} & \tau_{T_{\gamma_4}} \end{bmatrix} \tag{3.46}$$

3.3 COMPLIANT TENSEGRITY MECHANSIM GENERALIZATION

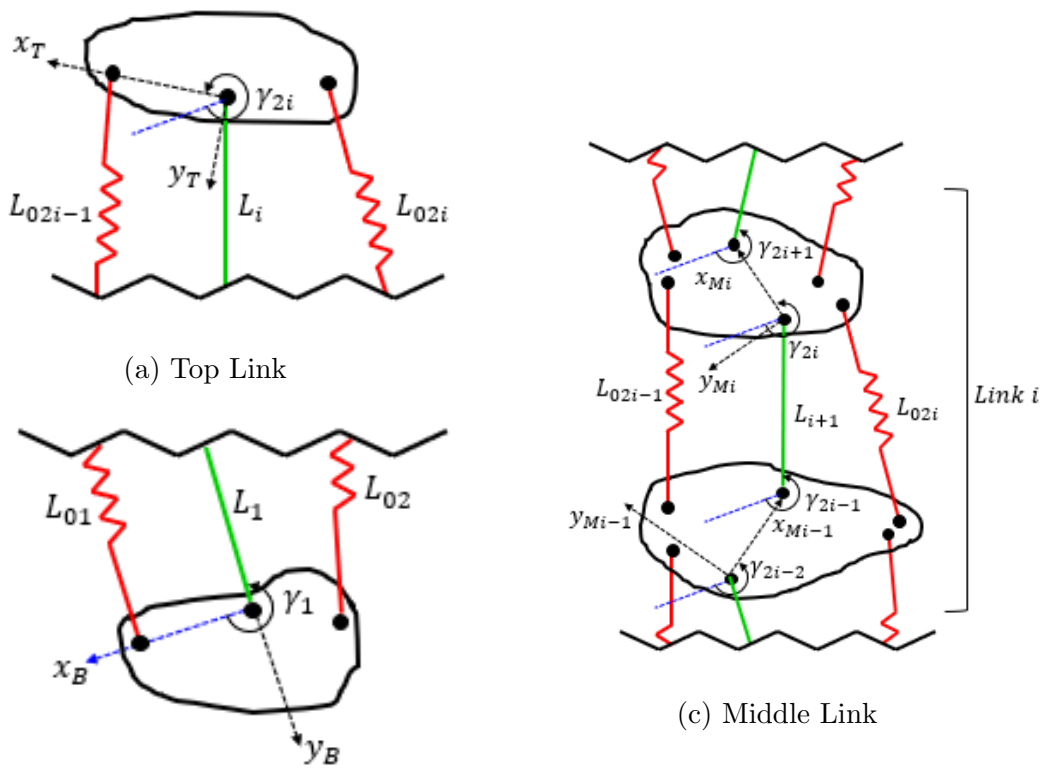

(a) Top Link

(b) Bottom Link

(c) Middle Link

Figure 3.3: General figures showing how the (a) top, (b) bottom and (c) middle links are defined for a CoTM

A CoTM can be broken down into three different types of links - top, middle and bottom - and each type of link is defined in a general manner as shown in Figure 3.3. It displays how the reference frames for each rigid body are defined, how each of the elements are named and how the angles that determine the overall orientation of the mechanism are

specified.

Every CoTM contains one bottom link, one top link and $i - 1$ middle links where i is the number of links in the chain. The only exception is for a single link CoTM, which has no middle links. For all mechanisms, the number of links are counted starting from the bottom as link 1, which is also shown in the generalized figure.

This setup for defining the mechanism facilitates convenient referencing/nomenclature and determination system equations (equilibrium, constraint) and variables. For example, for $i = 1$, the system of equations consists of 2 EE, 2 TCE and 2 DCE for a total of 6 equations and variables. For a system of i links, there will be $2i$ EE (force and torque equations for each link), $2i$ DCE (2 d_i for each link) and $2i$ TCE (2 γ_i for each link) for a system of size $6i \times 6i$. Following this method a three link chain would then consist of 6 EE, 6 DCE and 6 TCE with variables c_i, s_i, d_i for $i = 1 \ldots 6$.

As seen in developing the system of equations for a single-link and two-link chain, there is no compressive force within the EE. This is necessary to maintain a simplified and balanced system of equations for a stacked CoTM that reduces computation time for Bertini^{TM}.

CHAPTER 4

SIMULATION AND EXPERIMENT

Equation Setup The equations listed in Table 3.2 are symbolically solved in Wolfram Mathematica ™[12]. These equations are imported into a Python™file where numerical replacement of the experimental parameters can be performed, and the resulting set of equations is the input for the numerical algebraic solver. The automation of variation of parameters can be performed at this step. This flow of information is illustrated in Figure 4.1.

System Analysis Each free length is varied from 0 m to 0.09 m at an interval of 0.03 m, for a total of 256 different free length cases. The Python script substitutes the given experimental parameters found in Table 4.1 into the equations from Mathematica and creates an input file for Bertini ™. The Bertini ™solver outputs a text file that lists all the possible found solutions for c_i, s_i, d_i for $i = 1 \ldots 4$. The Python script reads this solution file and saves the data into an array. Using the raw data, it calculates $\gamma_1, \gamma_2, \gamma_3, \gamma_4, J_\gamma, J_{L_0}, \text{eig}[J]$ and evaluates the stability of the solution. The unknown parameters include $c_i, s_i \forall i = 1 \ldots 4$ instead of the desired γ_i. The γ_is are uniquely evaluated using

$$\gamma_i = \text{atan2}(s_i, c_i) = \begin{cases} \tan^{-1}\left(\frac{y}{x}\right) & x > 0 \\ \tan^{-1}\left(\frac{y}{x}\right) + \pi & x < 0, y \geq 0 \\ +\frac{\pi}{2} & x = 0, y > 0 \\ -\frac{\pi}{2} & x = 0, y < 0 \\ \text{undefined} & x = 0, y = 0. \end{cases} \tag{4.1}$$

Parameter	Value
L_1, L_2	0.125 m
L_3	0.048 m
p_{2x}	0.03 m
p_{3x}, p_{3y}	0, 0.04 m
p_{5x}, p_{5y}	0.02, -0.03 m
p_{6x}, p_{6y}	0.02 m
p_{8x}, p_{8y}	0.02 m
p_{9x}, p_{9y}	0.02, -0.03 m
p_{11x}, p_{11y}	0, -0.04 m
p_{12x}	0.03 m
k_1, k_2, k_3, k_4	42.05 $\frac{N}{m}$
$l_{01}, l_{02}, l_{03}, l_{04}$	0.065 m

Table 4.1: Experimental parameters used for study

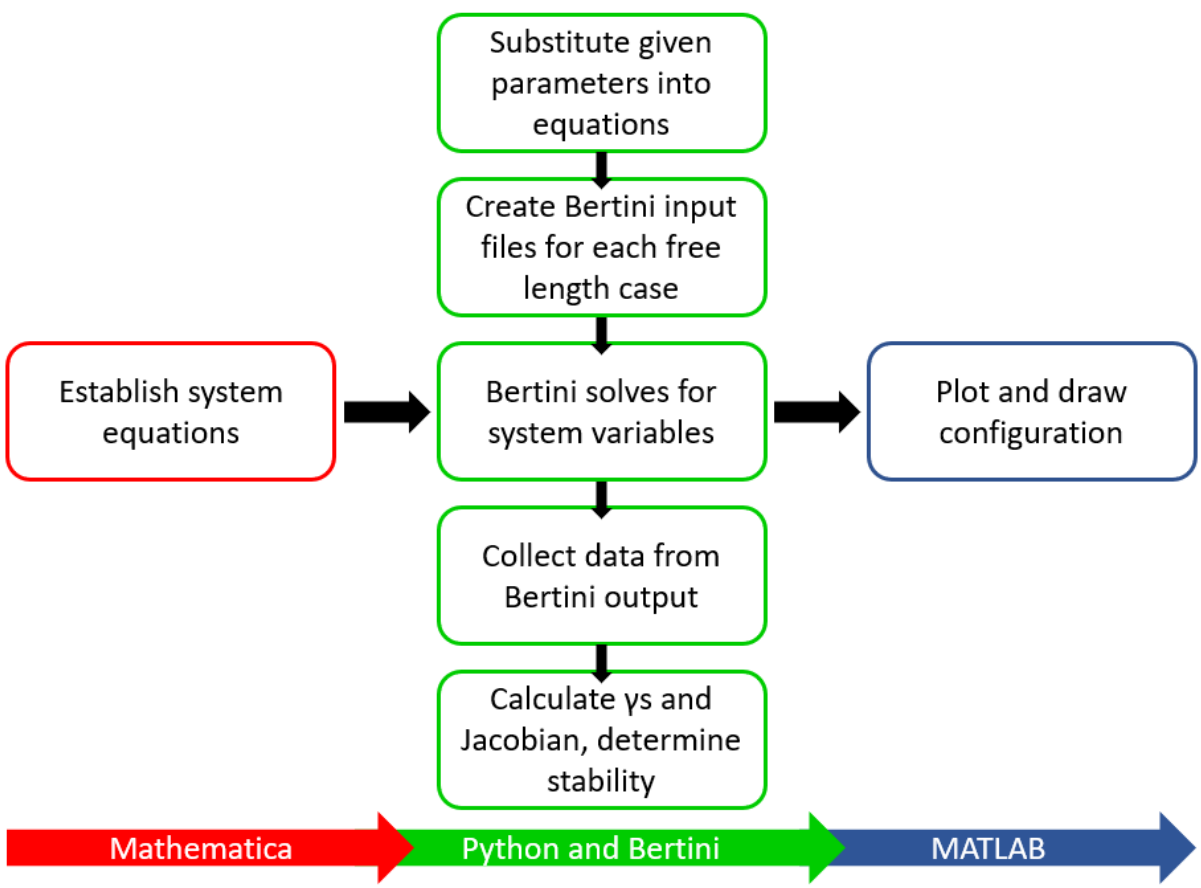

Figure 4.1: Flowchart of the simulation process to solve for a system of equations

All the system parameters, free lengths, raw data from Bertini and the calculated information is stored in an array. This process is repeated for all solutions and the array is output as a csv file.

Solution Analysis This csv file can be read into MATLAB™for analysis of the results. This involves plotting and drawing all the calculated solutions to observe how altering each of the free lengths affects the configuration, and comparison of the non-stable to stable solutions. Some stable solutions are shown in Figures 4.2 to 4.4 and the unstable solutions are shown in Figures 4.5 to 4.7. Detailed analysis of these results will be discussed in Section 5.

To verify results of the simulation, a physical model was built using the set parameters and the string length was varied and compared to the found results. These results will be further studied in Section 5.

All code is uploaded on the Agile Robotics Lab GitHub repository: https://github.com/UA-ARLhttps://github.com/UA-ARL.

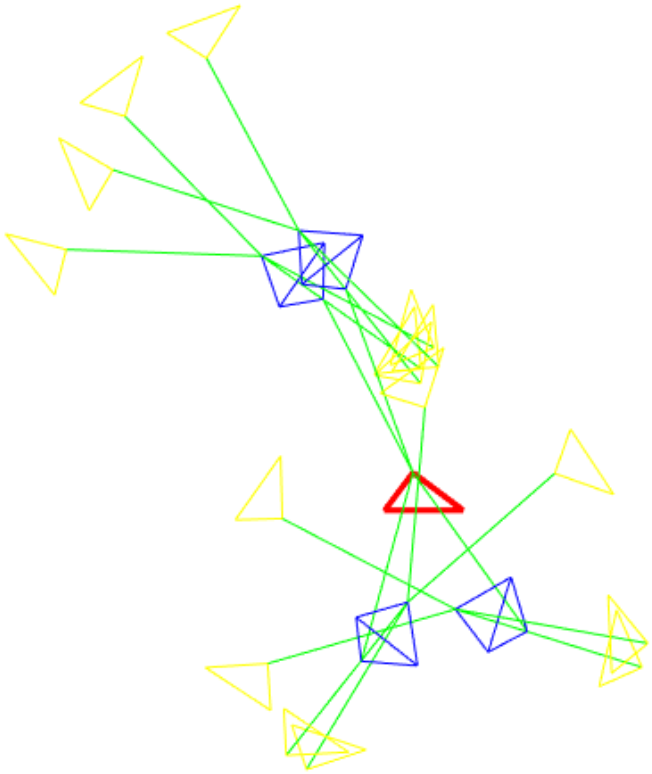

Figure 4.2: Visualization of stable solutions for $L_{01} = L_{02} = L_{03} = L_{04} = 0$ m where the bottom rigid body (red) is fixed and the middle body is marked in blue, the top rigid body is marked in yellow, and the two compressive members are marked in green.

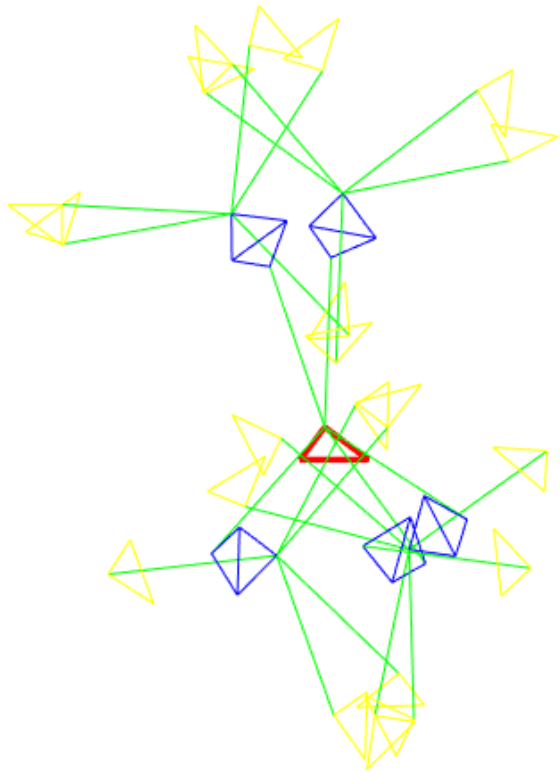

Figure 4.3: Visualization of stable solutions for $L_{01} = L_{02} = L_{03} = L_{04} = 0.09$ m where the bottom rigid body (red) is fixed and the middle body is marked in blue, the top rigid body is marked in yellow, and the two compressive members are marked in green.

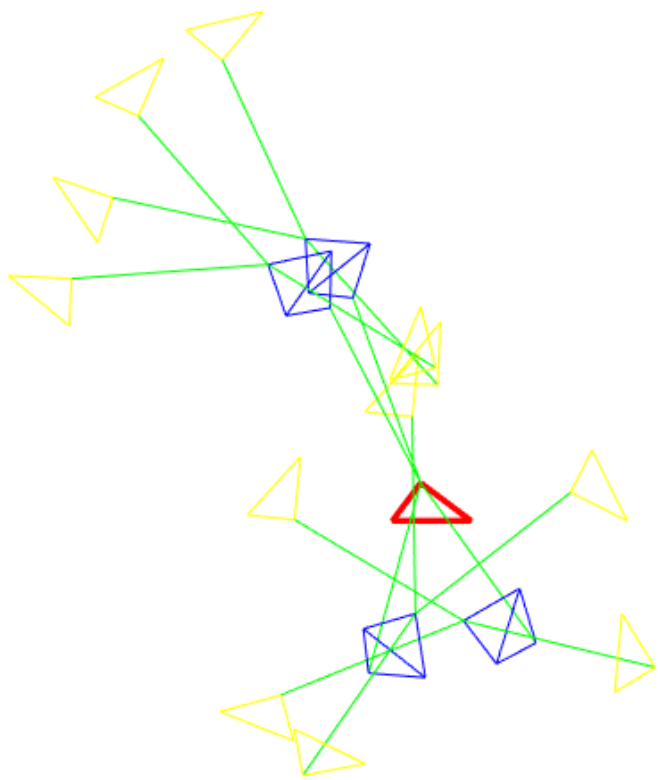

Figure 4.4: Visualization of stable solutions for $L_{01} = L_{02} = L_{04} = 0$ m and $L_{03} = 0.03$ m where the bottom rigid body (red) is fixed and the middle body is marked in blue, the top rigid body is marked in yellow, and the two compressive members are marked in green.

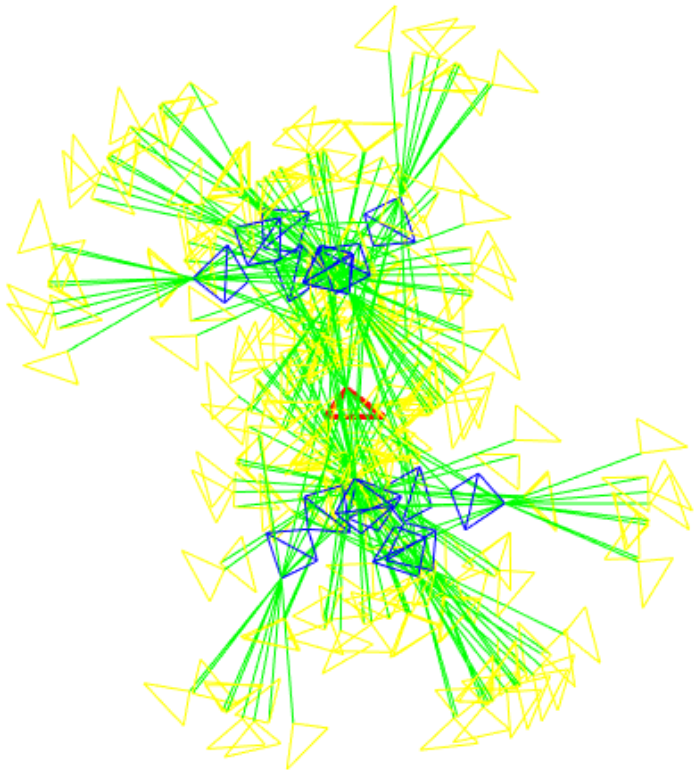

Figure 4.5: Visualization of unstable solutions for $L_{01} = L_{02} = L_{03} = L_{04} = 0$ m where the bottom rigid body (red) is fixed and the middle body is marked in blue, the top rigid body is marked in yellow, and the two compressive members are marked in green.

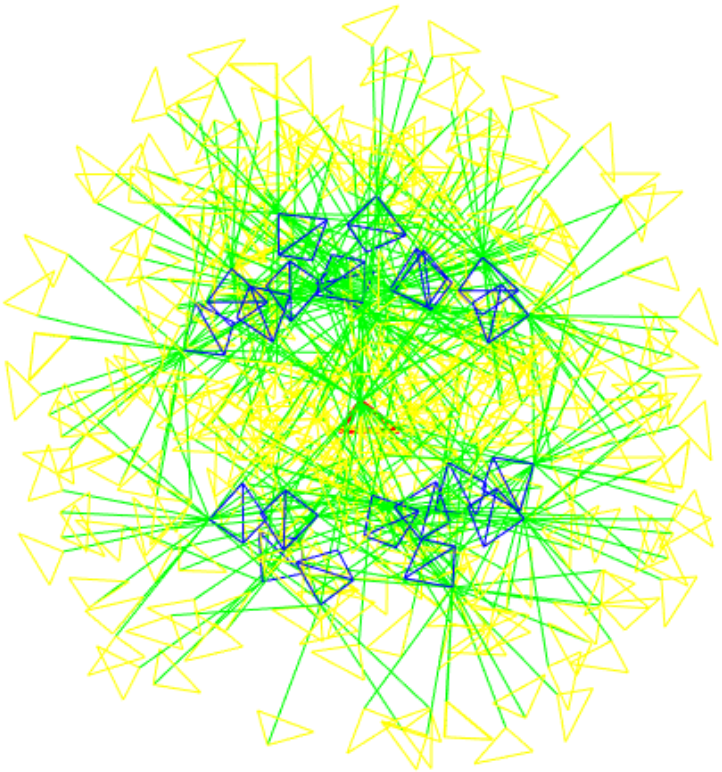

Figure 4.6: Visualization of unstable solutions for $L_{01} = L_{02} = L_{03} = L_{04} = 0.09$ m where the bottom rigid body (red) is fixed and the middle body is marked in blue, the top rigid body is marked in yellow, and the two compressive members are marked in green.

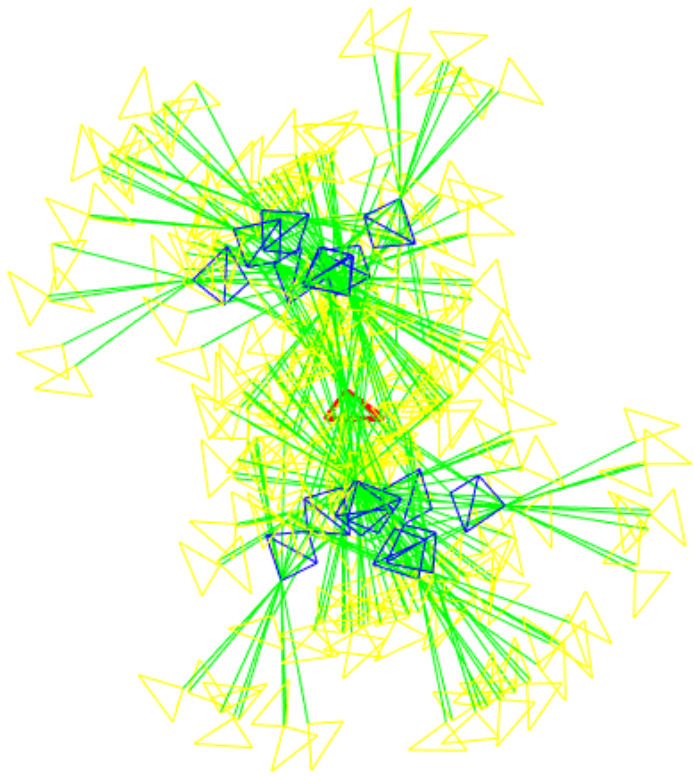

Figure 4.7: Visualization of unstable solutions for $L_{01} = L_{02} = L_{04} = 0$ m and $L_{03} = 0.03$ m where the bottom rigid body (red) is fixed and the middle body is marked in blue, the top rigid body is marked in yellow, and the two compressive members are marked in green.

CHAPTER 5

DISCUSSION

Theoretically, the equilibrium positions and their stability may be controlled through the spring free-lengths, L_{0i}s. However, the non-linearity of the mechanism introduces interesting non-intuitive behaviors. The overall simulation results are indicative of the setup of the equilibrium equations. For a two-link system, the kinematics of the top link (subsequently, the torque and force equations) is described using γ_1, γ_2, γ_3 and γ_4 while the equations for the bottom link only depend on γ_1 and γ_2. This trend is also apparent from Tables 3.1 and 3.2. These equations are setup as such because the mechanism is defined by the bottom body. Redefining the system from the top body instead would most likely incur the same trend, and the same results.

As mentioned earlier in Section 3.3, for a mechanism with i chains there needs to be $2i$ EEs that do not consider the unknown compressive force. If the compressive forces are considered, the system would become $7i \times 7i$ - $3i$ EEs, $2i$ DEs and $2i$ TCEs with two c_i, s_i, d_i and one f_i per link. While increasing the system by one may seem simpler, it actually severely increases complexity for Bertini^{TM} due to increase in number of variables. The decreasing of the complexity is achievable as system equations are linear in the compressive force. By eliminating this linear unknown and achieving a non-linear system of equations, the computation time for Bertini^{TM} to solve these systems is reduced, hence, none of the reduced EEs should contain the compressive forces.

For $i = 1$ and 2, this is simple as the overall force and torque equations can be manipulated easily to cancel out the compressive forces. However, this becomes more difficult

when mechanisms have $i > 2$ links. The EEs will then be taken in regards to the middle links, which are effected by two compressive forces rather than one. Future work will be based on determining the most efficient method for increasing the EEs in a chain of more than two links.

The change in two-link orientation is observed while only one control parameter (free-length L_{0i}) is varied while others are held constant (to zero in this case). The results are illustrated in Appendix A. The variation of free-lengths L_{01}, L_{02} results in a more robust control of orientation, while the orientations change more frequently upon change in L_{03}, L_{04}. From the simulation data shown in Section 4 and the Appendices A, B and C, it is clear to see that as the free lengths are varied the orientation of the mechanism changes, however, how drastically it does so is dependent on which free length is varied. This is true for both the stable and unstable solutions. In Appendix A, it is observed that the most change occurs when L_{02} is varied, most notably seen in Figures A.2, B.2 and C.2. The trend seems to show a tighter to looser formation as the free length is increased. Meaning, the solutions become less bunched together as the free length is increased. It is also seen that the stable solutions vary more when L_{01} and L_{02} are varied rather than varying L_{03} and L_{04}, and γ_2 shows the most variation of solutions. There are also fewer stable solutions as L_{01} and L_{02} are varied in comparison to varying L_{03} and L_{04}. This is probably due to their being multiple solutions for γ_3 and γ_4 for each solutions of γ_1 and γ_2. Although γ_1 and γ_2 are not affected as much by varying L_{03} and L_{04}.

From the data displayed in Appendices C and B, especially in Figures B.2 and C.2, it is clear that varying L_{02} shows the most effect on the mechanism orientation. However, this is unclear if it is due to these specific mechanism parameters, further study would need to observe the effect with more parameters to compare and see if the trend persists.

On the other hand, γ_3 and γ_4 solutions hardly vary as any of the free lengths are varied. Instead, as seen in figures of the configurations for different cases γ_3 and γ_4 seem to be more affected by changes in γ_1 and γ_2 rather than the free lengths. While unexpected,

this may be useful when looking for a solution close to a desired orientation. The potential solutions can be further narrowed down as it is now more limited by γ_1 and γ_2. The relationship between γ_1 and γ_2 with γ_3 and γ_4 are shown in Appendix D. From this data there seems to be a linear relationship between the angles as they increase. This could again be useful for mapping out desired orientations based on the bottom link. Future studies are needed to conclude whether or not this is a trend that continues as the chain grows. If it is, it may be possible for mechanism orientations to be designed based on the previous links orientation. In multi-link systems, such as chains much greater than two links, the mechanisms orientation could be broken down and looked at per pair of links. For instances of longer chains, this may not be as useful for design of the overall orientation, but could be advantageous if the objective was just to see how one part of the mechanism may change.

A physical model was built to verify results found. First, a model of a single link mechanism was built and the system was solved for two different cases of free length parameters as described in Section 3.1. Stable and unstable solutions for each case are shown in Figures 5.1a and 5.2a. Alongside (Figures 5.1b, 5.2b) are pictures of the physical model in one of the two stable configurations. A similar model was built for a two-link mechanism. An issue in the model that may cause this error, is a lack of tension throughout the spring elements. When the two-link model is setup with all free lengths at 0, issues arise from the springs being encumbered by the rigid body members, thus, limiting their movement. Due to these issues, the error seen between the results and physical model are attributed to poor model design. Future proposed designs for the model include placing the spring elements offset from the rigid body attached to a revolute joint, instead of a direct connection.

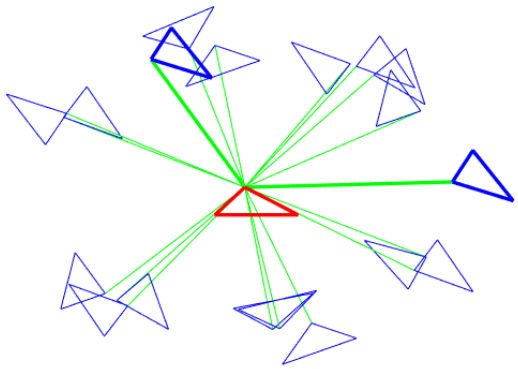

(a)

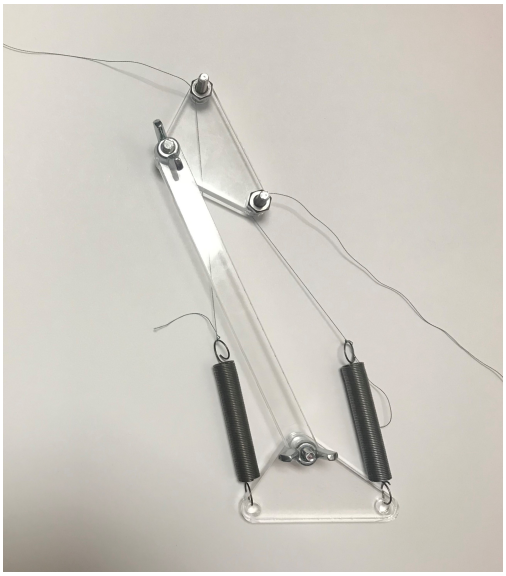

(b)

Figure 5.1: Physical verification of a single link CoTM, $L_{01} = 0.1, L_{02} = 0.065$ m. Two stable solutions were found and are highlighted in (a). One of the stable confiurations is shown with a physical model in (b).

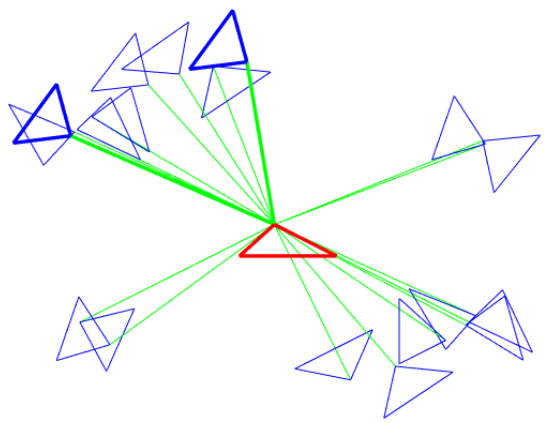

(a)

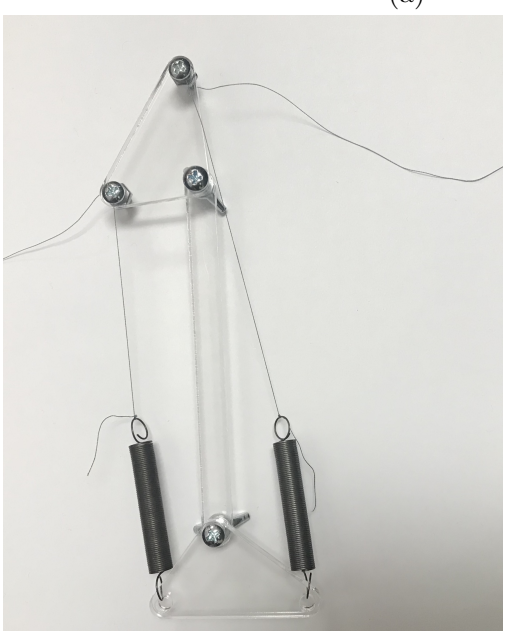

(b)

Figure 5.2: Physical verification of a single link CoTM, $L_{01} = 0.08, L_{02} = 0.13$ m. Two stable solutions were found and are highlighted in (a). One of the stable confiurations is shown with a physical model in (b).

CHAPTER 6

CONCLUSION

In conclusion, this work was able to present stacking of a planar compliant tensegrity mechanism and propose nomenclature (link orientation, unknowns) and form finding methodology. The form-finding methodology uses the force density method to find the the static equilibrium solutions and then determine the stability of those solutions. This is significant as not many have considered analyzing the stability of tensegrity mechanisms, or the analysis of compliant mechanisms either. Since CoTM are more robust than non-compliant tensegrity mechanisms they are a promising choice for further study and application in a variety of fields.

REFERENCES

[1] Marc Arsenault and Clment M. Gosselin. Kinematic, static and dynamic analysis of a planar 2-dof tensegrity mechanism. *Mechanism and Machine Theory*, 41(9):1072–1089, September 2006.

[2] Daniel J. Bates, Jonathan D. Hauenstein, Andrew J. Sommese, and Charles W. Wampler. Bertini: Software for numerical algebraic geometry. Available at bertini.nd.edu with permanent doi: dx.doi.org/10.7274/R0H41PB5.

[3] Nizar Bel Hadj Ali, Landolf Rhode-Barbarigos, Alberto A. Pascual Albi, and Ian F. C. Smith. Design optimization and dynamic analysis of a tensegrity-based footbridge. *Engineering Structures*, 32(11):3650–3659, November 2010.

[4] J. Bruce, K. Caluwaerts, A. Iscen, A. P. Sabelhaus, and V. SunSpiral. Design and evolution of a modular tensegrity robot platform. In *2014 IEEE International Conference on Robotics and Automation (ICRA)*, pages 3483–3489, May 2014.

[5] R. Connelly and W. Whiteley. Second-Order Rigidity and Prestress Stability for Tensegrity Frameworks. *SIAM Journal on Discrete Mathematics*, 9(3):453–491, August 1996.

[6] Carl D. Crane, Jahan Bayat, Vishesh Vikas, and Rodney Roberts. Kinematic Analysis of a Planar Tensegrity Mechanism with Pre-Stressed Springs. In Jadran Lenari and Philippe Wenger, editors, *Advances in Robot Kinematics: Analysis and Design*, pages 419–427. Springer Netherlands, Dordrecht, 2008.

[7] Arnoud A. T. M. Delissen, Giuseppe Radaelli, and Just L. Herder. Design and optimization of a general planar zero free length spring. *Mechanism and Machine Theory*, 117:56–77, November 2017.

[8] J Duffy, J Rooney, B Knight, and C D. Crane. A Review of a Family of Self-Deploying Tensegrity Structures with Elastic Ties. *The Shock and Vibration Digest*, 32:100–106, 2000.

[9] H. Furuya. Concept of deployable tensegrity structures in space application. *International Journal of Space Structures*, 7(2):143–151, 1992.

[10] Xinyang Geng, Marvin Zhang, Jonathan Bruce, Ken Caluwaerts, Massimo Vespignani, Vytas SunSpiral, Pieter Abbeel, and Sergey Levine. Deep reinforcement learning for tensegrity robot locomotion. *CoRR*, abs/1609.09049, 2016.

[11] Dawn Hustig-Schultz, Vytas SunSpiral, and Mircea Teodorescu. Morphological optimization for tensegrity quadruped locomotion. pages 3990–3995. IEEE, September 2017.

[12] Wolfram Research, Inc. Mathematica, Version 11.2. Champaign, IL, 2017.

[13] Donald E. Ingber. The architecture of life. *Scientific American*, 278(1):48–57, 1998.

[14] A. Iscen, A. Agogino, V. SunSpiral, and K. Tumer. Flop and roll: learning robust goal-directed locomotion for a tensegrity robot. In *IEEE/RSJ International Conference on Intelligent Robots and Systems*, pages 2236–2243, September 2014.

[15] Sergi Hernndez Juan and Josep M. Mirats Tur. Tensegrity frameworks: Static analysis review. *Mechanism and Machine Theory*, 43(7):859–881, July 2008.

[16] Deepak Kapur. Algorithmic Elimination Methods.

[17] Stephen M. Levin. The tensegrity-truss as a model for spine mechanics: biotensegrity. *Journal of mechanics in medicine and biology*, 2(03n04):375–388, 2002.

[18] Tim Liedl, Bjrn Hgberg, Jessica Tytell, Donald E. Ingber, and William M. Shih. Self-assembly of three-dimensional prestressed tensegrity structures from DNA. *Nature Nanotechnology*, 5(7):520–524, July 2010.

[19] Hidenori Murakami. Static and dynamic analyses of tensegrity structures. Part II. Quasi-static analysis. *International Journal of Solids and Structures*, 38(20):3615–3629, May 2001.

[20] Chandana Paul, Francisco J. Valero-cuevas, and Hod Lipson. Design and control of tensegrity robots for locomotion. *Ieee Transactions on Robotics*, 2006.

[21] A. Pugh. *An Introduction to Tensegrity*. The Dome series. University of California Press, 1976.

[22] M. Shibata, F. Saijyo, and S. Hirai. Crawling by body deformation of tensegrity structure robots. In *2009 IEEE International Conference on Robotics and Automation*, pages 4375–4380, May 2009.

[23] Gunnar Tibert. *Deployable tensegrity structures for space applications*. PhD Thesis, KTH Royal Institute of Technology, Sweden, 2002.

[24] Nicolas Veuve, Seif Dalil Safaei, and Ian F. C. Smith. Active control for mid-span connection of a deployable tensegrity footbridge. *Engineering Structures*, 112:245–255, April 2016.

[25] J.Y. Zhang and M. Ohsaki. Stability conditions for tensegrity structures. *International Journal of Solids and Structures*, 44(11):3875–3886, June 2007.

APPENDIX A

PLOTS OF L_{0I} VS γ_I FOR $I = 1...4$

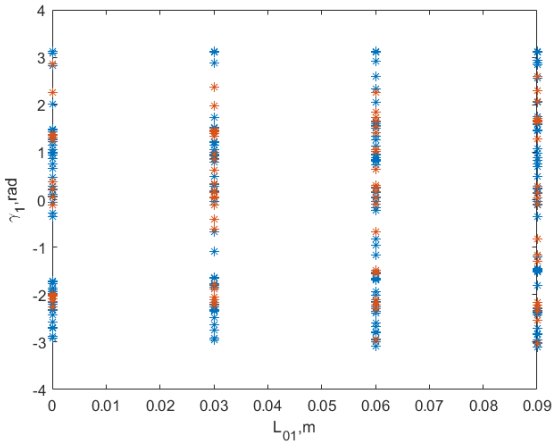

(a)

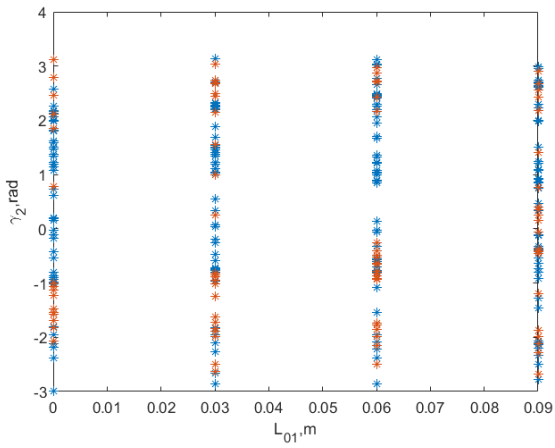

(b)

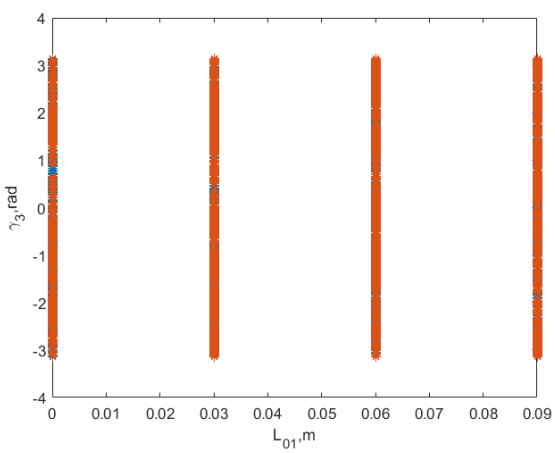

(c)

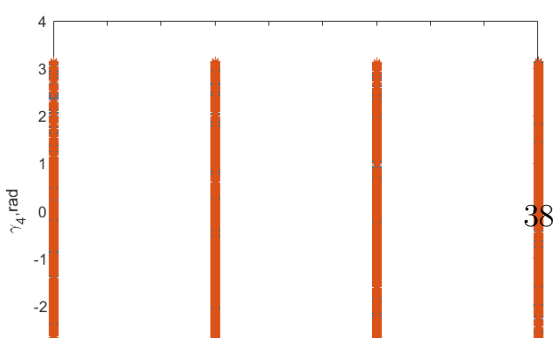

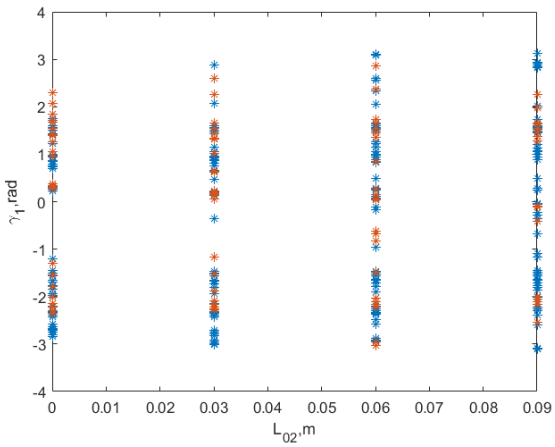

(a)

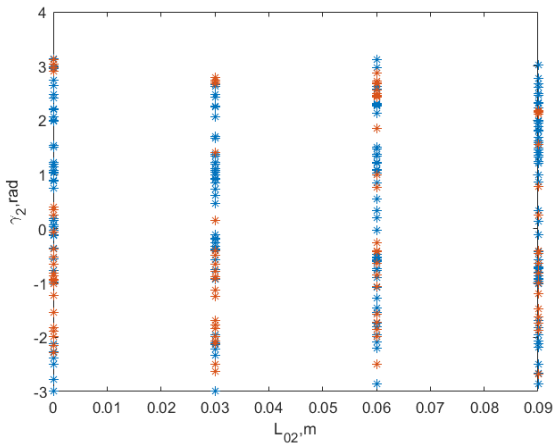

(b)

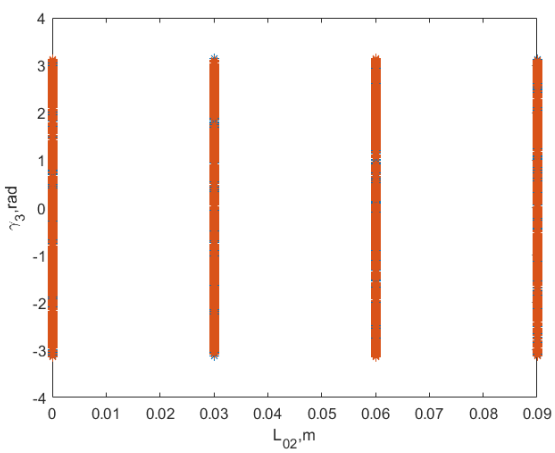

(c)

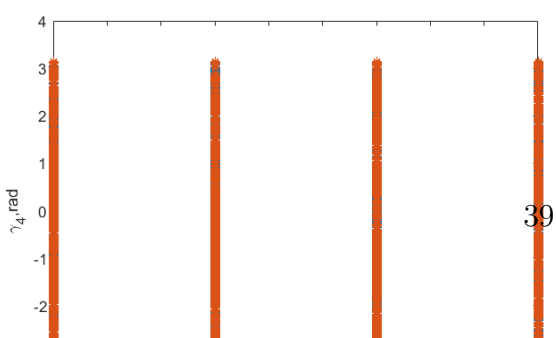

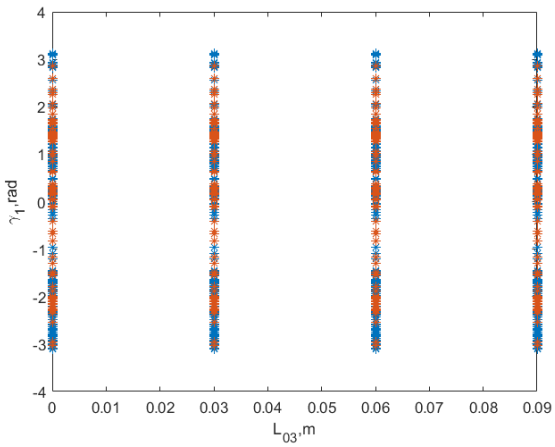

(a)

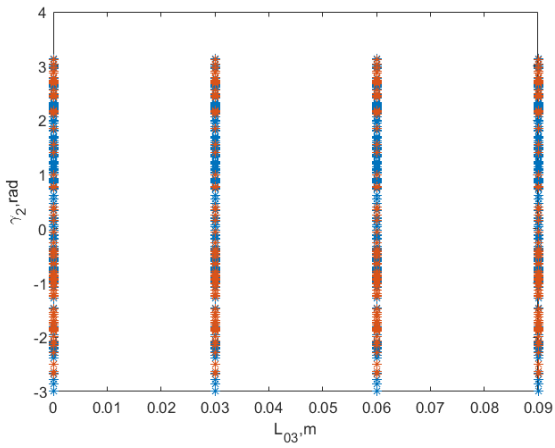

(b)

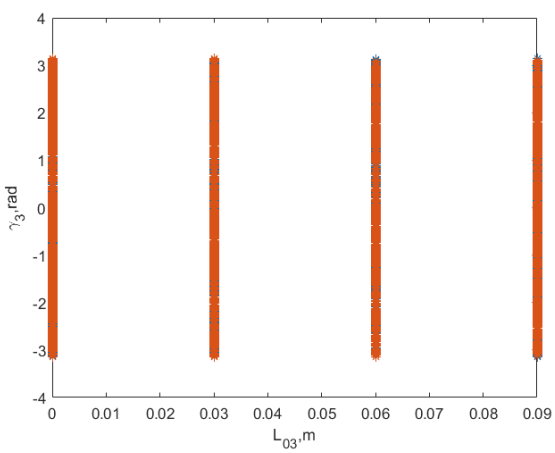

(c)

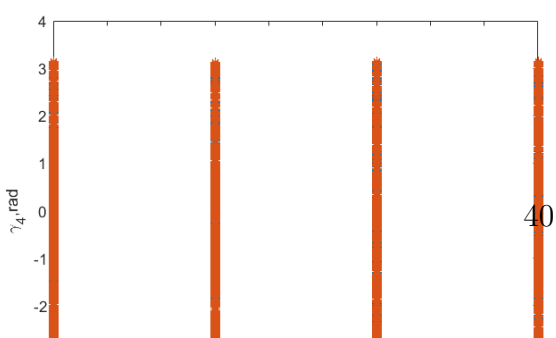

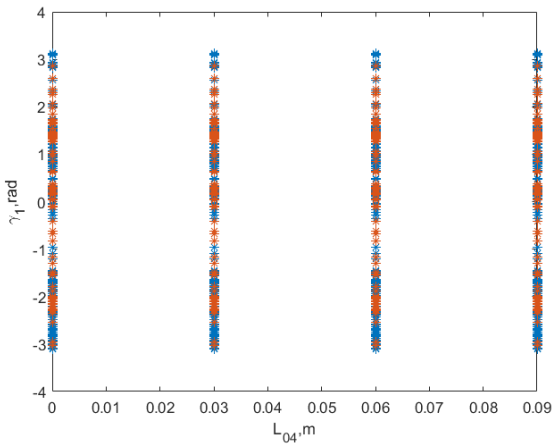

(a)

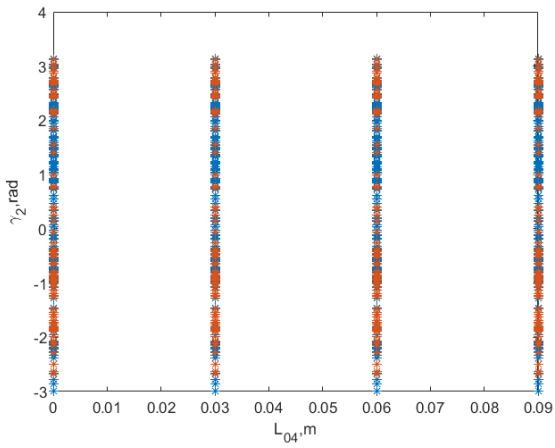

(b)

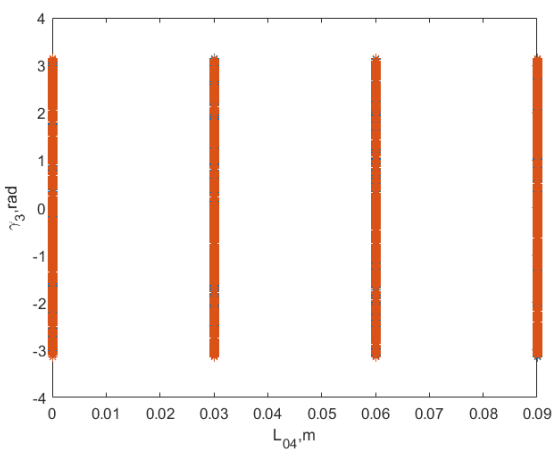

(c)

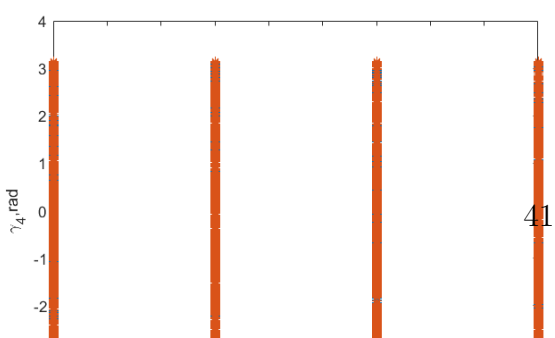

APPENDIX B

UNSTABLE MECHANISM ORIENTATION AS FREE LENGTHS ARE VARIED

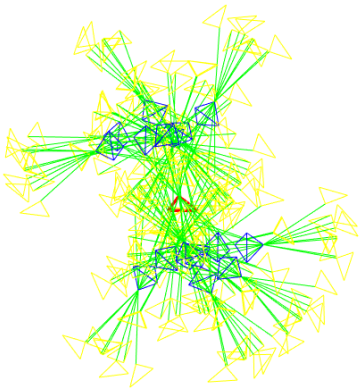

(a)

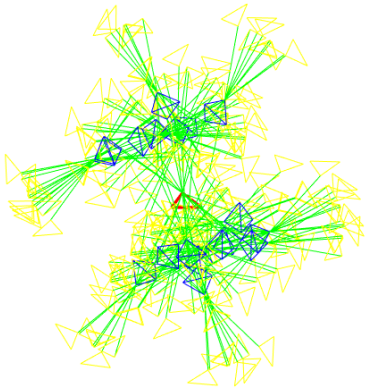

(b)

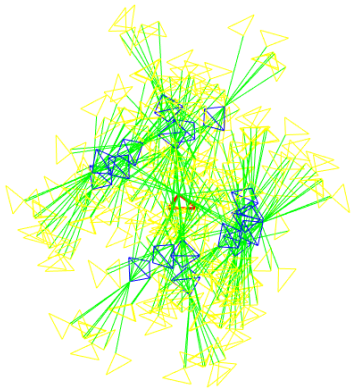

(c)

Figure B.1: Unstable orientation as $L_{02} = L_{03} = L_{04} = 0$ and L_{01} is varied from (a) 0.03 m, (b) 0.06 m to (c) 0.09 m

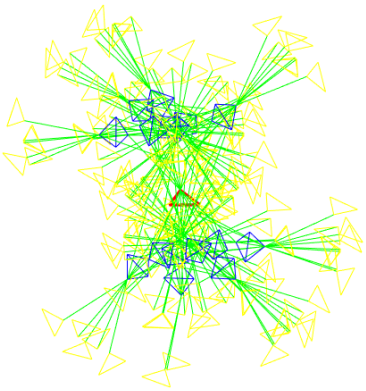

(a)

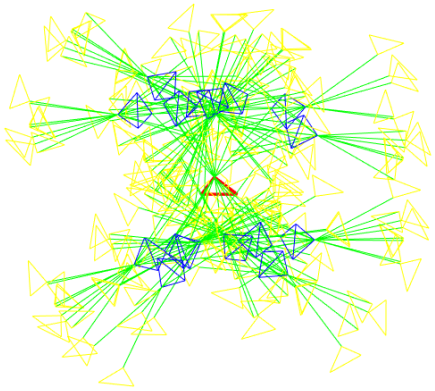

(b)

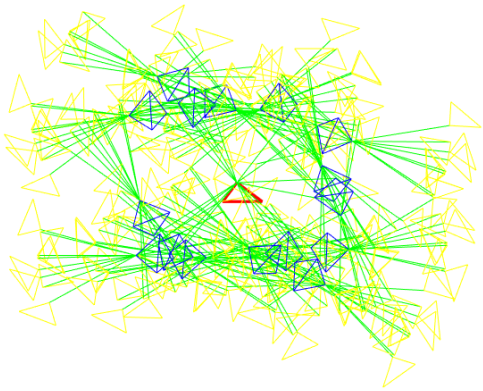

(c)

Figure B.2: Unstable orientation as $L_{01} = L_{03} = L_{04} = 0$ and L_{02} is varied from (a) 0.03 m, (b) 0.06 m to (c) 0.09 m

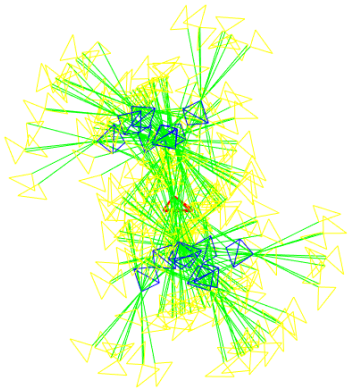

(a)

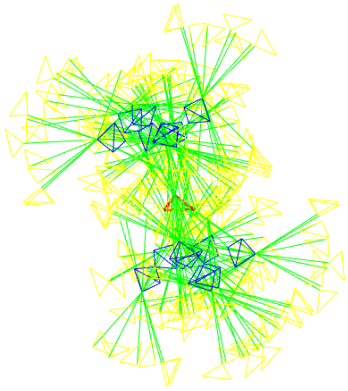

(b)

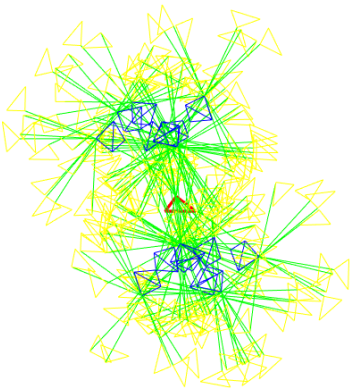

(c)

Figure B.3: Unstable orientation as $L_{01} = L_{02} = L_{04} = 0$ and L_{03} is varied from (a) 0.03 m, (b) 0.06 m to (c) 0.09 m

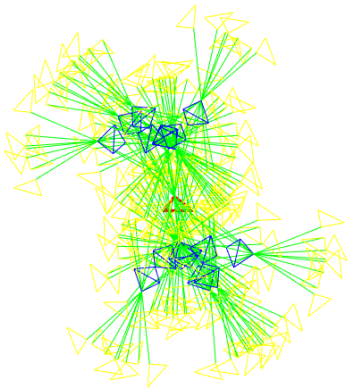

(a)

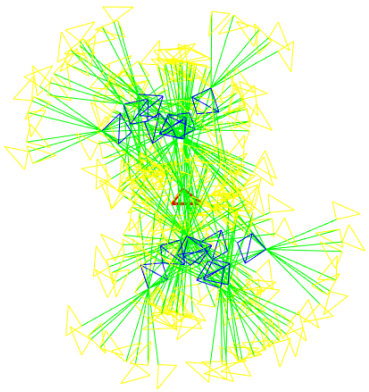

(b)

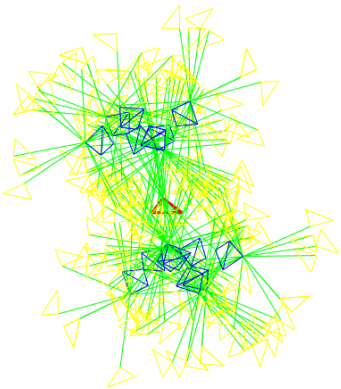

(c)

Figure B.4: Unstable orientation as $L_{01} = L_{02} = L_{03} = 0$ and L_{04} is varied from (a) 0.03 m, (b) 0.06 m to (c) 0.09 m

APPENDIX C

STABLE MECHANISM ORIENTATION AS FREE LENGTHS ARE VARIED

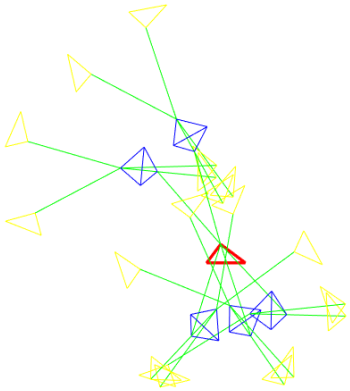

(a)

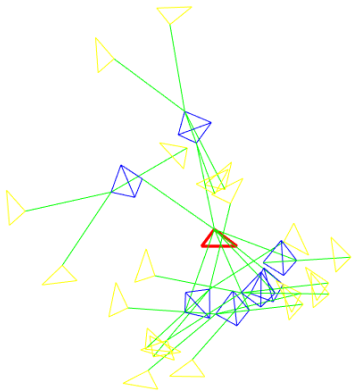

(b)

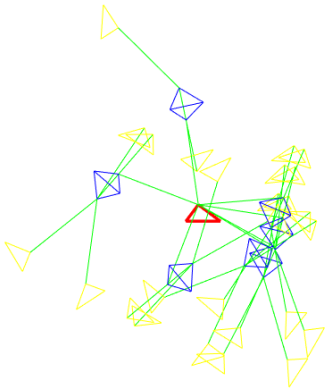

(c)

Figure C.1: Stable orientation as $L_{02} = L_{03} = L_{04} = 0$ and L_{01} is varied from (a) 0.03 m, (b) 0.06 m to (c) 0.09 m

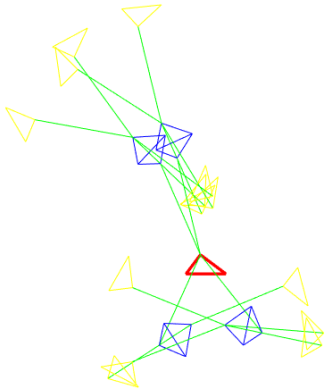

(a)

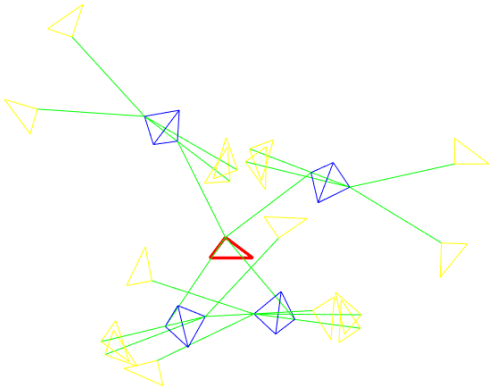

(b)

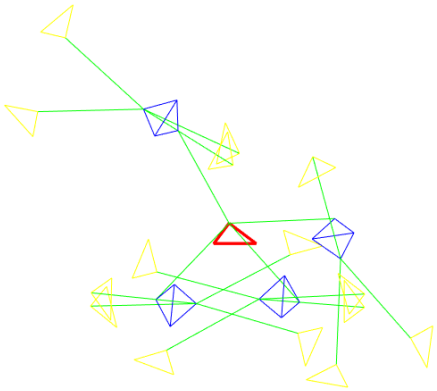

(c)

Figure C.2: Stable orientation as $L_{01} = L_{03} = L_{04} = 0$ and L_{02} is varied from (a) 0.03 m, (b) 0.06 m to (c) 0.09 m

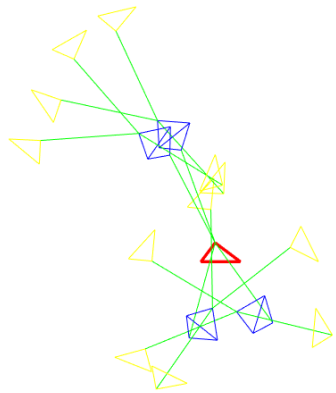

(a)

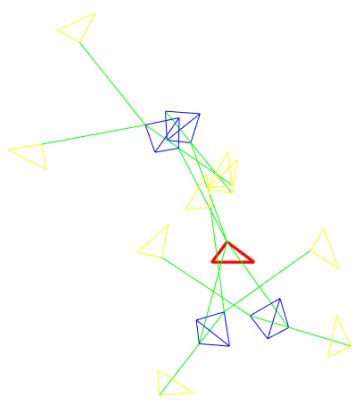

(b)

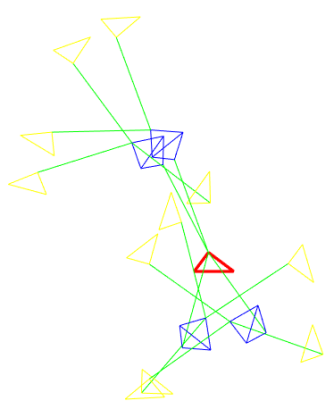

(c)

Figure C.3: Stable orientation as $L_{01} = L_{02} = L_{04} = 0$ and L_{03} is varied from (a) 0.03 m, (b) 0.06 m to (c) 0.09 m

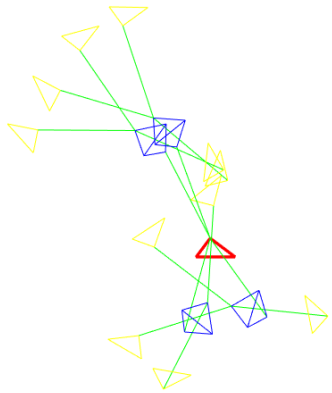

(a)

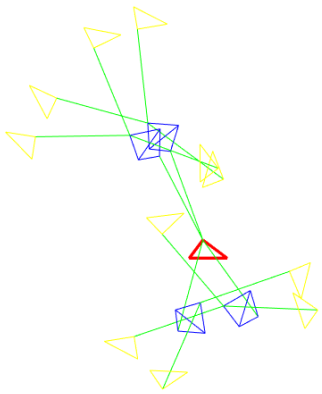

(b)

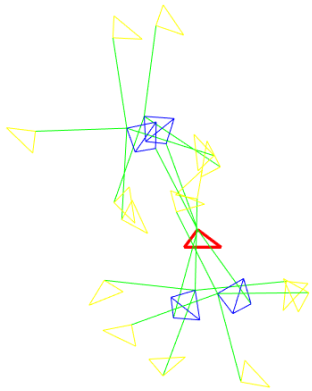

(c)

Figure C.4: Stable orientation as $L_{01} = L_{02} = L_{03} = 0$ and L_{04} is varied from (a) 0.03 m, (b) 0.06 m to (c) 0.09 m

APPENDIX D

PLOTS OF γ_1 AND γ_2 VS γ_3 AND γ_4

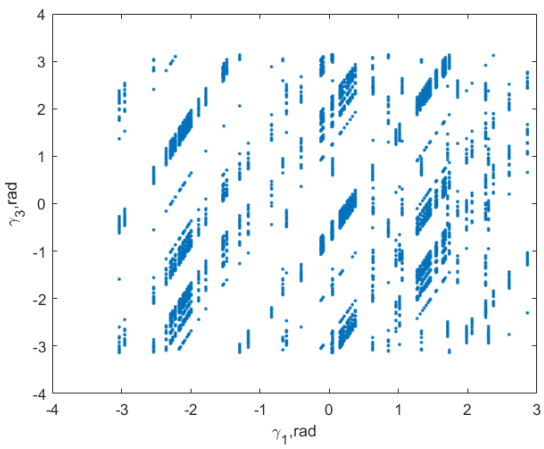

(a) Stable

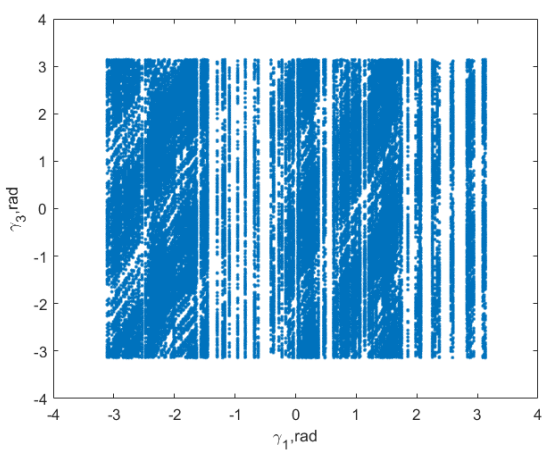

(b) Unstable

Figure D.1: Variation of γ_3 as γ_1 is increased.

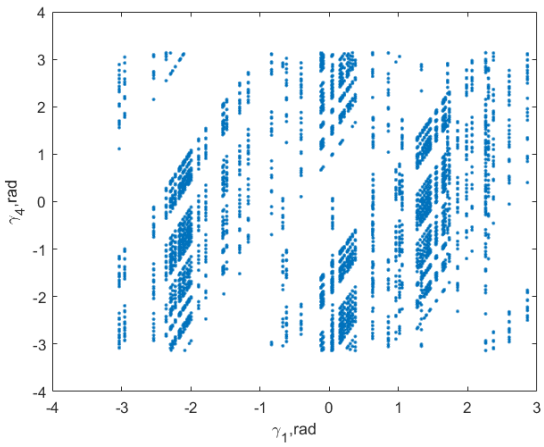

(a) Stable

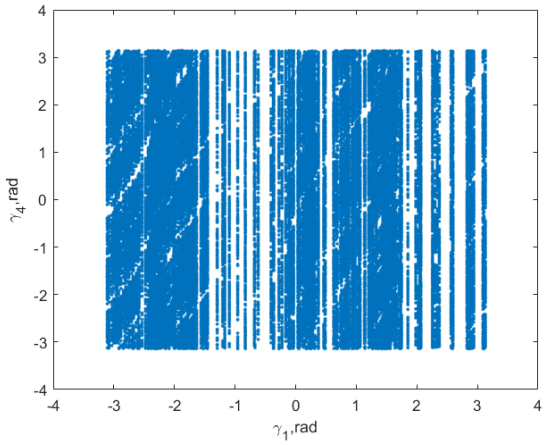

(b) Unstable

Figure D.2: Variation of γ_4 as γ_1 is increased.

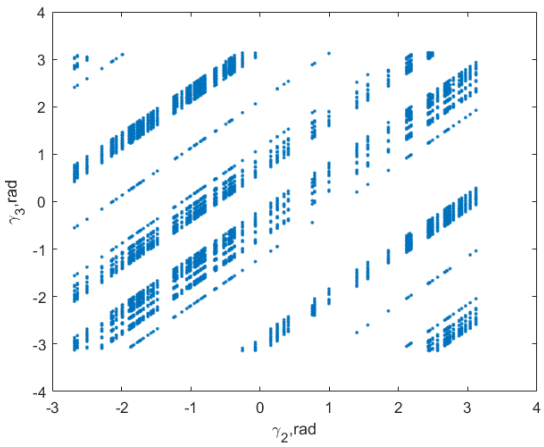

(a) Stable

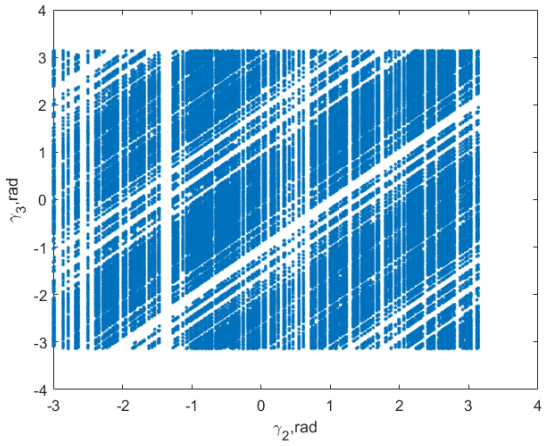

(b) Unstable

Figure D.3: Variation of γ_3 as γ_2 is increased.

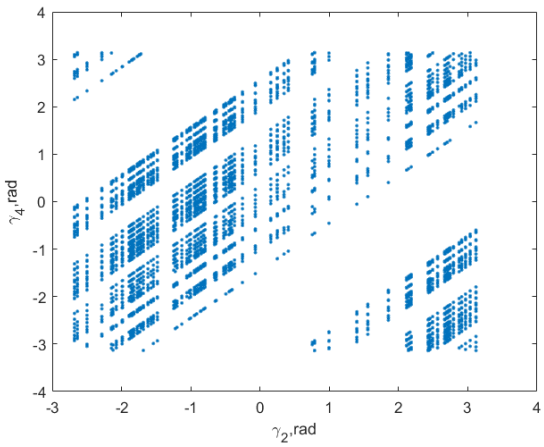

(a) Stable

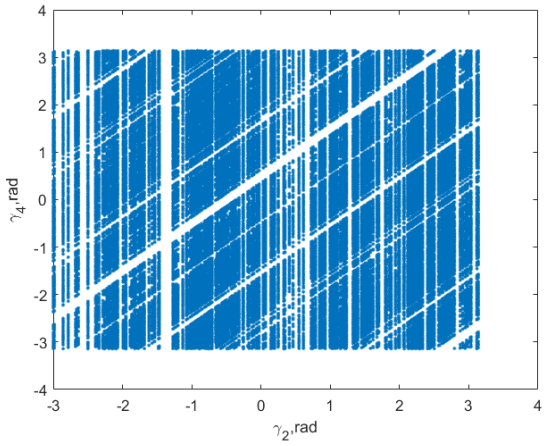

(b) Unstable

Figure D.4: Variation of γ_4 as γ_2 is increased.